



Development of a sEMG-Based Joint Torque Estimation Strategy Using Hill-Type Muscle Model and Neural Network

Dawen Xu¹ · Qingcong Wu^{1,2} · Yanghui Zhu¹

Received: 17 March 2020 / Accepted: 1 June 2020 / Published online: 8 June 2020
© Taiwanese Society of Biomedical Engineering 2020

Abstract

Purpose Exoskeleton control based on motion intention recognition has received increasing attention due to its promising prospect, and estimating joint torque is an effective approach to conduct intention recognition. In this paper, a surface electromyography (sEMG) signals-based joint torque estimation strategy is proposed to quantify the motion intention.

Methods Different from the majority of existing torque estimation strategies, two major improvements have been achieved. System identification is presented to estimate elbow angle which can be used in the Hill-type muscle model, and hence, the use of angular transducer is replaced. Besides, neural network is used to train the optimal factor of muscle activation to make the estimated torque more accurate. Finally, static and dynamic experiments are conducted respectively to verify the effectiveness and improvements of this strategy in terms of torque estimation accuracy.

Results Compared to the other two existing torque estimation strategies, results show that this method is proved to make some progress in respect of torque estimation accuracy under different experimental conditions. The correlation coefficient increases by 2–9%; root-mean-square error (RMSE) reduces by 0.2–2.5 Nm; normalized root-mean-square error (NRMSE) reduces by 0.5–9.5%.

Conclusion The proposed torque estimation strategy could accurately identify the motion intention and reduce the use of angle sensor. Besides, it lays a foundation for rehabilitation exoskeleton robot control.

Keywords Intention recognition · Torque estimation strategy · sEMG · Hill-type muscle model · Radical basis function neural network (RBFNN)

1 Introduction

With the increasing number of hemiplegic patients and demands for machine-assisted rehabilitation, varieties of rehabilitation exoskeleton robots have been developed for assistance [1–4]. In order to efficiently control robots, the first challenge is to recognize human motion intention in

a rapid and accurate way. Recognition of human motion intention based on biological signals [5–7] has become increasingly popular due to its promising prospect in human–computer interaction. For the different expression forms of motion intention, existing recognition methods mainly include the forms of physiological signals, such as surface electromyography (sEMG) signals, neural signals, including electroencephalogram (EEG) signals, and such biological force signals, as human–computer interaction force signals.

Compared with other signals, sEMG signals are widely used in the robotic systems to obtain human motion intention due to its effectiveness, safety, portability and non-invasive, non-delay features [8, 9]. In order to improve patients' muscle coordination and exercise ability, the sEMG signals have been introduced as driving or feedback signals into the rehabilitation process for the elderly, stroke patients or others in need [10–12]. Previous researchers show that estimating joint torque is one of the effective approaches to realizing

✉ Qingcong Wu
wuqc@nuaa.edu.cn

Dawen Xu
xudawen@nuaa.edu.cn

Yanghui Zhu
zhuyanghui@nuaa.edu.cn

¹ College of Mechanical and Electrical Engineering, Nanjing University of Aeronautics and Astronautics, Nanjing 210016, Jiangsu Province, China

² Jiangsu JWC Machinery CO.,LTD, HuaiAn 211600, Jiangsu Province, China

intention recognition [13]. Hence, it is necessary to propose a joint torque estimation method based on sEMG signals to realize intention recognition and then continuously controlling the robots.

Existing joint torque estimation methods can be listed as follows [14–17]. Cai [14] estimated the knee torque using Support Vector Regression (SVM) which required a large amount of matrix storage and computation, thus a large amount of machine memory and operation time were consumed. Besides, it was difficult to implement this algorithm for large-scale training samples. Researchers [15, 17] established various non-linear relationships between sEMG and joint torque, which didn't take human muscle models into account. Tyler et al. [16] put forward a complex muscle activation model, including neural activation dynamics, muscle activation dynamics, muscle contraction dynamics, muscle moment arms and skeletal motion model. Obviously, too many human parameters needed to be identified, and complex functional relationships between variables needed to be established, which complicated the operation process and limited the application to robot controlling.

In prior research, the joint angle was often utilized to estimate joint torque. Angle was measured by different sensors in traditional methods [17, 18]. However, the application of the angle sensors not only brought the installation problems for exoskeleton robots, but also often needed complicated algorithms to figure out the angle. Aiming at the problems mentioned above, researchers have done lots of research on the angle estimation [19–21]. Zhang [19] used a feedforward artificial neural network model to make the mapping from sEMG to the elbow joint angle. Principle component analysis (PCA) or independent component analysis (ICA) was used in the process of feature extraction. Researchers [20–22] used Back-Propagation neural network (BPNN) and RBFNN to acquire the relationship between the sEMG and joint angle. The input, output and other parameters of the neural network needed to be set before the training which complicated the estimation process. Therefore, it is necessary to develop a relatively simple and accurate angle estimation strategy to ensure the estimation accuracy and simplify the operation.

In this paper, a sEMG-based joint torque estimation strategy combining with Hill-type muscle model (HMM) by using RBFNN and system identification is proposed to make the results of muscular movement digitized. Elbow joint angle is estimated through a transfer function model which interpreted a non-linear relationship. RBFNN is used to get the optimal factor of muscle activation, making the estimated joint torque more accurate. Compared to the existing torque estimation strategy, this method not only improves the estimation accuracy but also replaces the angle sensors. Finally, static and dynamic experiments based on these three different methods are conducted to prove that

the improvements of this new strategy in terms of torque estimation accuracy.

2 Method

The joint torque estimation strategy will be carried out in several steps, which involve the processing of sEMG signals, system recognition and neural networks. This method will be introduced in two parts as follows. One is the joint angle estimation strategy, and the other is the muscle activation and muscle model.

2.1 Joint Angle Estimation Strategy

In order to replace the angle transducer and optimize the process of angle estimation, a new joint estimation angle method that establishes a relationship between sEMG and the joint angle is presented in this paper. A transfer function model is built up to relate sEMG signals from the biceps brachii to the joint angle. Furthermore, system identification is applied to estimate the parameters of the transfer function model, which only focuses on the input and output values. In this way, only a few calibration tests need to be done and simplify the hardware in practical application.

The entire process of angle estimation strategy is described in Fig. 1. In order to obtain high-quality required sEMG signals, a series of processing steps are adopted, part of which can refer to the paper [17, 23]. In this research, the biceps brachii is selected as the main responsible muscle of the elbow joint [24, 25]. Before collecting sEMG signals by the sEMG sensor (MyoWare Sensor), the muscle's surface must be cleaned with alcohol cotton to remove grease and stains. The fine hairs on the surface of the human body need to be removed with special cutting tools to ensure the high-quality original signals. Next, the sEMG sensor is put on the center of muscle and it should be mounted parallel to the direction of muscle fiber [26]. In addition, due to the influences of noise and other interference factors, the original sEMG signals are not suitable for direct application, so it must go through a series of filtering and rectification operations.

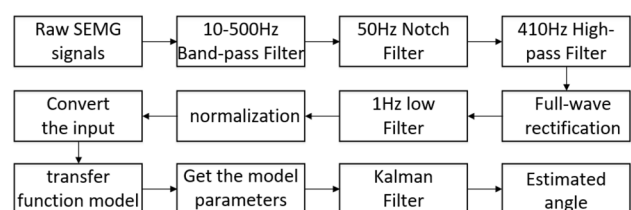


Fig. 1 The procedure of the angle estimation strategy

Besides, data amplitude is susceptible to several factors, such as electrodes location, subjects or even mental condition and so on. Normalizing sEMG data to 0–1 can solve some of these problems. Hence, after 1 Hz low-pass filter, the sEMG signals should be normalized with regard to the amplitude of sEMG.

Furthermore, in order to make the low amplitude increase of sEMG more obvious during the slow motion, the input signals of the transfer function model can be computed from the normalized sEMG signals, and the corresponding relationship can be described as shown below:

$$v(t) = -\frac{1}{\ln(u(t))} \tag{1}$$

where

$$0 < u(t) < 1 \tag{2}$$

Here, $v(t)$ is the input signals of transfer function model and $u(t)$ is the normalized sEMG signals. This research presents a relationship between the sEMG and the joint angle, which can be defined as follows:

$$G(s) = \frac{v(s)}{\theta(s)} = \frac{k(1 + T_zs)}{(1 + T_{p1}s)(1 + T_{p2}s)(1 + T_{p3}s)} \tag{3}$$

where $G(s)$ is the transfer function; $v(s)$ is the input signals of this model and it is the Laplace transform of the processed sEMG $v(t)$; $\theta(s)$ is the output signals of this model and it is the Laplace transform of the elbow joint angle $\theta(t)$; s is a complex variable; $k, T_z, T_{p1}, T_{p2}, T_{p3}$ are all coefficients in this transfer function model. Moreover, the parameters of the transfer function are different under different load conditions. Also, all the coefficients can be obtained through system identification module in the Host personal computer (PC).

Usually, the signals obtained after these processing steps also contain gaussian white noise. Therefore, Kalman filtering is used to remove gaussian white noise and smooth the signals.

2.2 The Muscle Activation and Muscle Model

In this part, sEMG signals could be transformed into muscle activation through a series of processing, and then combined with the muscle model and neural network to obtain the estimated torque of the elbow joint.

2.2.1 From the sEMG Signals to the Muscle Activation

Some of the preprocess of sEMG has been described above and the following operations will be discussed in the following part. The operation procedure of torque estimation

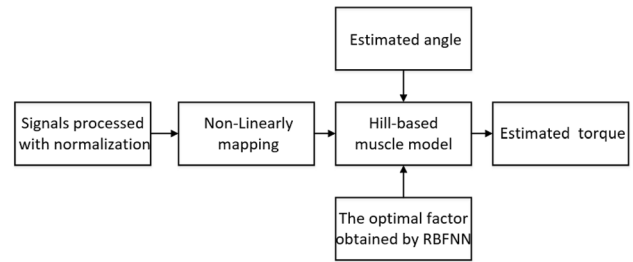


Fig. 2 The procedure of elbow joint torque estimation strategy

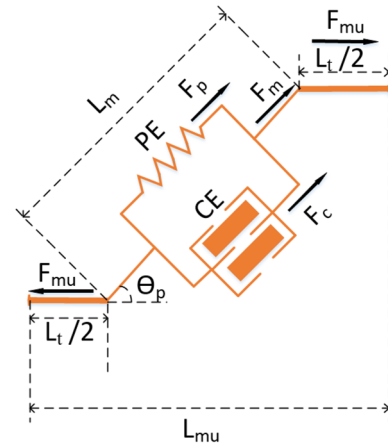


Fig. 3 Hill-based muscle model (HMM). It contains a number of elements, that is PE parallel elastic element; CE contractile element; F_{mu} force of the muscletendon unit; F_m force of muscle fiber; F_c force of contractile element; F_p force of parallel elastic element; L_t length of tendon; L_m length of muscle fiber; L_{mu} length of the muscletendon unit; θ_p pennation angle

strategy is illustrated in Fig. 2. In this research, a model is proposed to characterize the non-linear relationship between sEMG level and muscle activation on the basis of the theory reported in the article [27], which can be expressed as:

$$a(t) = \frac{1}{q} \cdot \frac{e^{A \cdot u(t)} - 1}{e^A - 1} \tag{4}$$

where $u(t)$ is the normalized sEMG signals; $a(t)$ is muscle activation; A is a constant determining the degree of non-linearity; q is a variable parameter that will be trained in the RBFNN, also its specific meaning and expression method will be explained in formula (17).

2.2.2 From Muscle Activation to the Estimated Torque

The muscle activation could be obtained through Eq. (4) and then used to compute the muscle force. This model, described in Fig. 3, has gone through many times of evolution and simplification. The picture illustrates that a muscle–tendon unit

contains a contractile element (CE), a passive element (PE) and tendons. The force F_{mu} produced by the muscle–tendon unit can be given as [28]:

$$F_{mu} = (F_c + F_p) \cdot \cos(\theta_p) \tag{5}$$

where F_{mu} represents the force generated by the muscle–tendon unit; F_c is the force generated by the contractile element; F_p denotes the force generated by the passive element; θ_p is the Pennation angle. Force generated by CE and PE can be given by the following equations:

$$F_c = f_c(l_m) \cdot f_c(v_m) \cdot a(t) \cdot F_{mo} \tag{6}$$

$$F_p = f_p(l_m) \cdot F_{mo} \tag{7}$$

Here, $a(t)$ is muscle activation; F_{mo} represents the maximum isometric muscle force; $f_c(l_m)$ and $f_c(v_m)$ indicate the force–length and force–velocity relationship for the CE, respectively, while $f_p(l_m)$ represents the force–length relationship for the PE. In order to calculate F_{mu} , these relationships can be defined by the following equations:

$$f_c(l_m) = \begin{cases} r_0 \cdot \left(\frac{L_m}{L_{mo}}\right)^2 + r_1 \cdot \frac{L_m}{L_{mo}} + r_2, & 0.5 \leq \frac{L_m}{L_{mo}} \leq 1.5 \\ 0, & \text{otherwise} \end{cases} \tag{8}$$

$$f_c(v_m) = 1 \tag{9}$$

$$f_p(l_m) = e^{10 \cdot \frac{L_m}{L_{mo}} - 15} \tag{10}$$

where L_m is the muscle fiber length and L_{mo} represents the optimal fiber length; r_0 , r_1 , and r_2 are set to be the constants.

The following formula can be derived from Fig. 3:

$$L_{mu} = L_t + L_m \cdot \cos(\theta_p) \tag{11}$$

Here, L_t is the length of the tendons and L_{mu} is the musculo-tendinous unit length. To simplify the calculation process, the following assumptions are made according to the article [27]:

$$L_{mu} = \eta + \mu \cdot \theta_e \tag{12}$$

$$\tau = F_{mu} \cdot \mu \tag{13}$$

where τ is the joint moment at time t ; θ_e is the estimated joint angle; η and μ are constants. Many body parameters can be referred to the previous research [28–31]. The parameters mentioned above are shown in Table 1. In this research, the whole experiment will be conducted in two ways, i.e. the static and dynamic experiments, as shown in Figs. 4 and 5, respectively.

Experimental setup for static experiment is shown in Fig. 4. In this case, the upper arm is always perpendicular to the lower arm. The hand pulls the wire rope and the force should be completely generated by the biceps brachii. A tension sensor (JLBS-MD-10KG) is utilized to measure the tension during the experiment. The actual torque can be calculated through this formula:

$$\tau_{a1} = F_t \cdot r_a \tag{14}$$

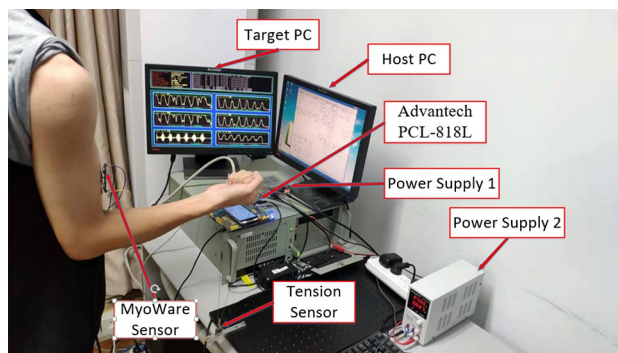


Fig. 4 System layout in the static experiment

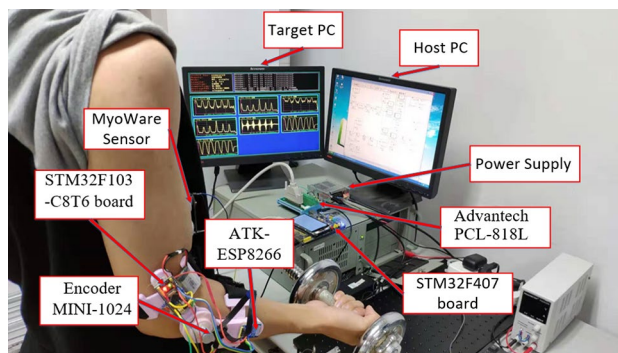


Fig. 5 System layout in the dynamic experiment

Table 1 Definition and values of parameters

| Parameter name | Value |
|---|--------------------|
| Maximum isometric muscle force F_{mo} | [435.6 N, 624.3 N] |
| Optimal fiber length L_{mo} | [0.116 m, 0.132 m] |
| Length of tendon L_t | [0.192 m, 0.272 m] |
| Pennation angle θ_p | 0 |
| Length of the lower arm r_a | 0.33 m |
| Mass of the lower arm G_2 | 30 N |
| Constant r_0 | – 2.06 |
| Constant r_1 | 6.16 |
| Constant r_2 | – 3.13 |
| Nonlinear coefficient A | 0.05 |

where τ_{a1} represents the actual torque in the static case, F_t represents the force generated by the tension sensor, r_a is the length of the lower arm.

Experimental setup for dynamic case is shown in Fig. 5. The upper arm should always be perpendicular to the ground throughout the experiment. The hand lifts the bar and the force is completely generated by the biceps brachii too. In the dynamic experiment, the actual torque can be calculated roughly according to the formula (15), and the calculation model is shown in Fig. 6.

$$\tau_{a2} = r_a \cdot F = \left(G_1 + \frac{G_2}{2} \right) \cdot r_a \cdot \sin \theta \quad (15)$$

where τ_{a2} represents the actual torque in the dynamic experiment; G_1 is the mass of the barbell; G_2 represents the mass of the lower arm; θ is the angle of the elbow joint; F is the force perpendicular to the ground. In both cases, muscle activation $a_j(t)$ can be deduced through the actual torque and HMM. Moreover, the muscle activation mentioned in the article [27] is described as:

$$a_2(t) = \frac{e^{A \cdot u(t)} - 1}{e^A - 1} \quad (16)$$

Here, $u(t)$ is the normalized sEMG signals. Lots of experiment results show that there is a deviation between $a_1(t)$ and $a_2(t)$. Therefore, q is used to describe this relationship, which can be described as:

$$q = \frac{a_2(t)}{a_1(t)} \quad (17)$$

According to the paper [32], RBFNN is a kind of local approaching neural networks, which is often used to handle non-linear control. What's more, compared with other neural networks, RBFNN has some sound characteristics, such as

high approximation accuracy and fast training speed. Therefore, RBFNN will be used to get the real-time parameter q in this paper.

Generally speaking, RBFNN has three layers [33], namely input layer, hidden layer and output layer. The input layer is used to receive all elements which have strong correlations with the output results, and passes them to the hidden layer. The hidden layer performs multivariate nonlinear transformation on the input vector for feature extraction. The output layer is trained by the model to determine the output weights of neurons in each hidden layer, then outputs the weights after linear combination. The relationships between the three layers can be expressed by the following two formulas:

$$y = \sum_{i=1}^n w_i h_i \quad (18)$$

$$h_i = \exp \left\{ - \frac{\|x - c_i\|^2}{2 \cdot b_i^2} \right\} b_i i_{th} \quad (19)$$

where x and y are the input and output, respectively; w_i represents the weights for the node i from the hidden layer to the output layer, $i=1,2,3,\dots,n$; h_i is the activation function for hidden layer. c_i and b_i are the parameters of basis function and its width for i_{th} node in the hidden layer.

The training process of RBFNN can be roughly divided into two stages. Firstly, the center of the activation function for the hidden layer is selected. In RBFNN, self-organized center selection is the most widely used learning algorithm and orthogonal least square method is the most commonly utilized self-organized center selection method. Therefore, the orthogonal least square method is chosen to select the center. Furthermore, the Gram–Schmidt algorithm is used to select and update the center. Next, determine the output weights of neurons in each hidden layer. Adaptive gradient descent is used to adapt the weights. All the values of RBFNN can be acquired when the output errors meet the requirements. In this paper, muscle activation $a_2(t)$, Normalized sEMG $u(t)$, elbow joint angle $\theta(t)$ and raw sEMG $r(t)$ are selected as the inputs of the neural network [34], while q is the output of the neural network. The inputs of neural network are in conformity with the following principles. One is that all inputs have certain impacts on the output. The other is that the numbers of inputs should not be too small and the comprehensive effects could make the output more accurate. The structure of the RBFNN is shown in Fig. 7.

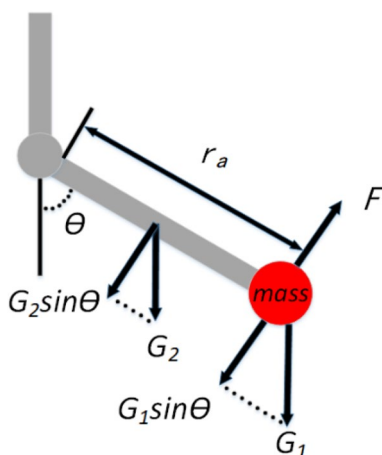


Fig. 6 The actual torque calculation model in the dynamic experiment

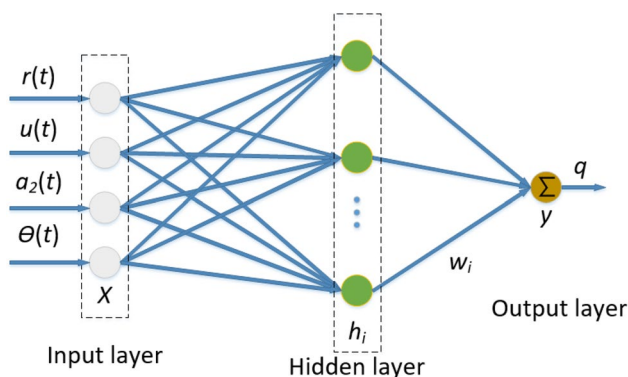


Fig.7 Schematic diagram of neural network

3 Experimental Setup

In this research, a healthy male adult, aged 23, height 180.5 cm, weight 68 kg, has participated in the experiments. The employed experimental methods of this paper have been approved by the Institutional Review Board of Nanjing University of Aeronautics and Astronautics.

As stated above, this paper will verify the feasibility of the torque estimation strategy in static and dynamic cases. In the static case, just as shown in Fig. 4, the experimenter stands by the experimental platform, keeping the upper and lower arms perpendicular, and pulls the tension sensor by the biceps brachii. The force signals are collected by the tension sensor (JLBS-MD-10KG). In the dynamic case, just as demonstrated in Fig. 5, the experimenter holds barbells of different mass, raising and laying down them at a constant rate with different frequencies. The experiments are conducted at different frequencies (1/2 Hz, 1/3 Hz and 1/4 Hz) and loads (0 kg, 3 kg and 5 kg). Elbow angle is provided by the encoder (MINI-1024 ATI Industrial Automation) and angle calculation algorithm is carried out in the microcontroller (ALIENTEK STM32F103C8T6). The angle signals are sent to the development board (ALIENTEK STM32F407) through the WIFI module (ATK-ESP8266) and then transmitted to the Target PC. Finally, the relationship between the sEMG and the joint angle will be established in System identification module in the Host PC. The experimenter takes a 3-min break to relieve muscle fatigue after each test. Moreover, to avoid electromagnetic interference, the unnecessary motors and machines are removed.

Considering the correlation coefficient between estimated joint torque and measured joint torque, the validity of estimated joint torque can be measured as follows:

$$\rho_{T_a, T_e} = \frac{Cov(T_a, T_e)}{\sigma_{T_a} \cdot \sigma_{T_e}} \tag{20}$$

where T_a and T_e represent the actual joint torque and estimated joint torque; Cov defines the covariance. In addition, σ_{T_a} and σ_{T_e} indicate the standard deviation of actual and estimated joint torque. Apart from that, in order to calculate the error between the actual joint torque and the estimated joint torque, root mean square error (RMSE) and normalized root mean square error (NRMSE) are taken into account [17], which are shown as:

$$RMSE = \sqrt{\frac{\sum_{t=1}^N (T_{at} - T_{et})^2}{N}} \tag{21}$$

$$NRMSE = \frac{RMSE}{T_{et\max} - T_{et\min}} \tag{22}$$

where N is the number of joint torque data; T_{at} , T_{et} are the actual joint torque and estimated joint torque at time t . $T_{et\max}$, $T_{et\min}$ represent the maximum and minimum of T_{et} .

4 Experiments and Analysis

Results of the static case are shown in Fig. 8. Considering the contingency in a single experiment, three experiments are conducted under the static condition in search of a more general conclusion. The measuring standards ρ , $RMSE$ and $NRMSE$ in each experiment are listed in Table 2. The results of experimental methods (Method 1–3) proposed in this research and the articles [17, 28] are shown successively. In the Method 2, the researcher used the IMU to get the joint angle and did not consider the optimal factor in the process of getting muscle activation while the method just established a non-linear relationship between the sEMG and joint torque in the Method 3.

In the static experiments, the average correlation coefficient between actual joint torque and estimated joint torque obtained by Methods 1, 2 and 3 are 97.88%, 95.90% and 94.86%, respectively. The results show that the estimated joint torque calculated by Method 1 has better correlations with the actual joint torque than that by Methods 2 and 3. In addition, according to the pictures (c) in three trials, the estimated torque obtained by Method 1 is highly in accordance with the trend of actual torque, demonstrating that Method 1 can identify the variation like muscle changes, which cannot be accomplished by Methods 2 and 3. The average RMSE between actual joint torque and estimated joint torque obtained by Methods 1, 2 and 3 are 1.447 Nm, 3.908 Nm and 5.714 Nm, respectively. The average NRMSE between actual joint torque and estimated joint torque obtained by Methods 1, 2 and 3 are 5.446%, 9.200% and 14.574%, respectively. Besides, according to the pictures (d) in three trials, errors obtained by Method 1 are mainly focus on the range of ± 4

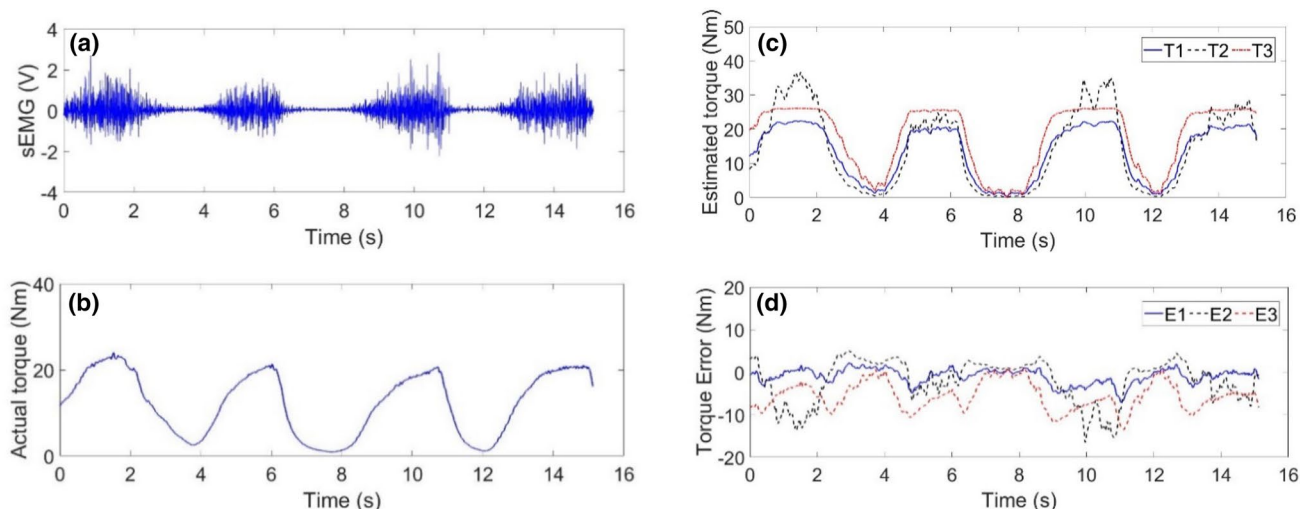


Fig. 8 Above are relevant experimental data in the first experiment. T1, T2, T3 represent the estimated torque obtained by Methods 1, 2 and 3, respectively. E1, E2, E3 represent errors between actual torque and estimated torque obtained by Methods 1, 2 and 3, respectively. **a**

Raw sEMG signals **b** Actual torque **c** Estimated torque obtained by three estimation strategies **d** Errors between actual torque and three different estimated torques

Table 2 Comparisons of the experimental results obtained by methods 1, 2, 3 (M1, M2, M3) in the three experiments

| | ρ (%) | | | RMSE (Nm) | | | NRMSE (%) | | |
|---------|------------|-------|-------|-----------|-------|-------|-----------|-------|--------|
| | M1 | M2 | M3 | M1 | M2 | M3 | M1 | M2 | M3 |
| Trial 1 | 97.67 | 95.42 | 94.98 | 1.016 | 3.039 | 3.502 | 5.932 | 9.081 | 14.723 |
| Trial 2 | 98.31 | 95.53 | 95.69 | 1.767 | 4.061 | 6.128 | 4.534 | 9.984 | 13.512 |
| Trial 3 | 97.66 | 96.74 | 93.91 | 1.559 | 4.623 | 7.511 | 5.873 | 8.537 | 15.488 |
| Average | 97.88 | 95.90 | 94.86 | 1.447 | 3.908 | 5.714 | 5.446 | 9.200 | 14.574 |

Nm, which are acceptable. Plus, errors obtained by Method 1 are smaller than that by Methods 2 and 3, which indicates that at most time, estimated joint torque obtained by Method 1 is closer to actual joint torque than that by Methods 2 and 3. In conclusion, in the static experiment, Method 1 has a better performance than Methods 2 and 3.

In the dynamic case, experiments have been conducted three times at each frequency and load. The results of the dynamic experimental method under 0 kg, 3 kg and 5 kg are shown in Figs. 9, 10 and 11, respectively. Moreover, the average values of ρ , RMSE and NRMSE at different frequencies (1/2 Hz, 1/3 Hz and 1/4 Hz) and loads (0 kg, 3 kg and 5 kg) are recorded in Tables 3, 4 and 5.

Just as the pictures (b) shown in Figs. 9, 10 and 11, the estimated angle and actual angle have positive correlations, and the errors between the actual and estimated angle are smaller enough to be accepted. Tables 3, 4 and 5 show that the estimated torque obtained by Method 1 has a better correlation with the actual torque than that by Methods 2 and 3. Except that, RMSE and NRMSE calculated by Method 1 are smaller than that by Methods 2 and 3 at most of time, which means the accuracy of estimated torque obtained by Method

1 is higher compared to the other two methods. Results show that compared to the other two existing torque estimation strategies, this method is proved to make progress in the aspect of torque estimation accuracy under different experimental conditions. The correlation coefficient increases by 2–9%; root-mean-square error (RMSE) reduces by 0.2–2.5 Nm; normalized root-mean-square error (NRMSE) reduces by 0.5–9.5%. Moreover, under the same load condition, the performances at high frequency (1/2 Hz) are better than low frequency (1/4 Hz) while worse than moderate frequency (1/3 Hz); at the same frequency, the performances under 0 kg are slightly worse than moderate load (3 kg) condition and better than the big load (5 kg). Two main reasons can explain these two phenomena. Firstly, the degree of muscle activation is relatively low as the experimenter lifts the low-mass barbell at a low speed, resulting in relatively poor estimation accuracy. The other is that the bigger the load is, the longer the load time is, the more energy the experimenter consumes, and the greater possibility of muscle shaking and fatigue. It requires that the torque estimation strategy can accurately detect the muscle condition in a very short time and make the corresponding changes, which is no doubt a

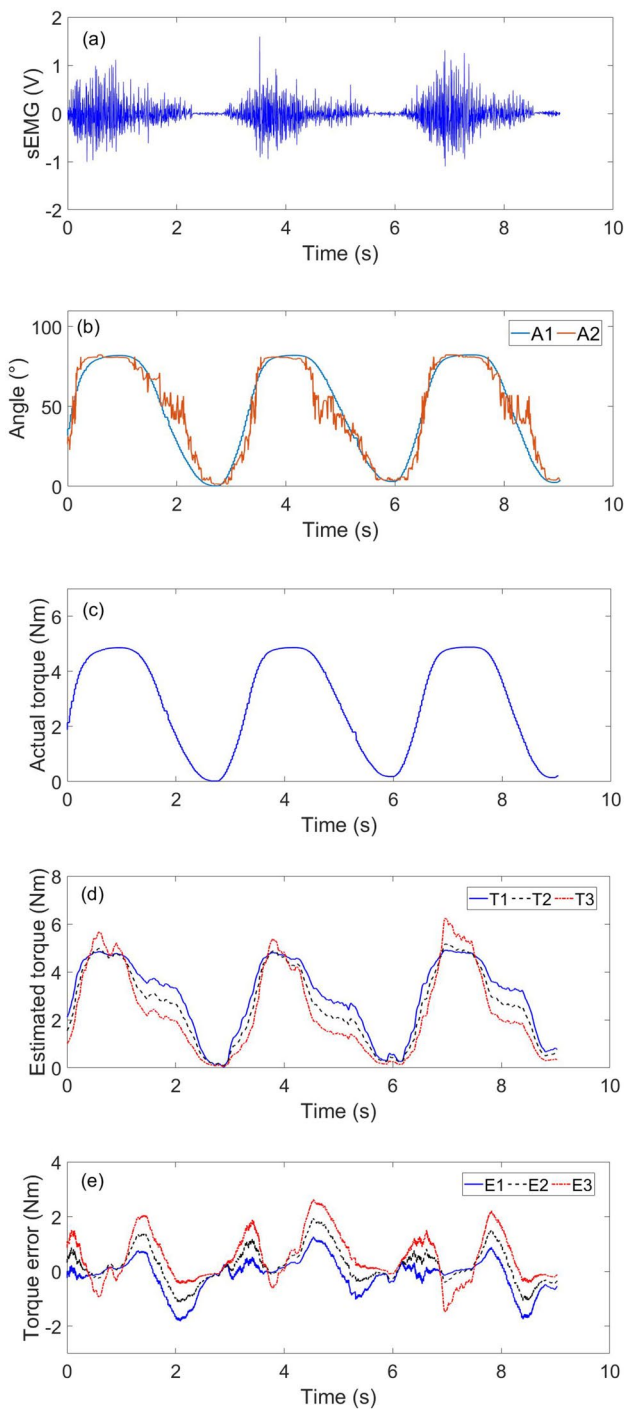


Fig. 9 Above are experimental results under no load condition. T_1 , T_2 , T_3 represent the estimated torque obtained by Methods 1, 2 and 3, respectively. E_1 , E_2 , E_3 represent errors between actual torque and estimated torque obtained by Methods 1, 2 and 3, respectively. A_1 , A_2 are the actual angle and the estimated angle; **a** Raw sEMG signals **b** Actual angle and estimated angle **c** Actual torque **d** Estimated torque obtained by three estimation strategies **e** Errors between actual torque and three different estimated torques

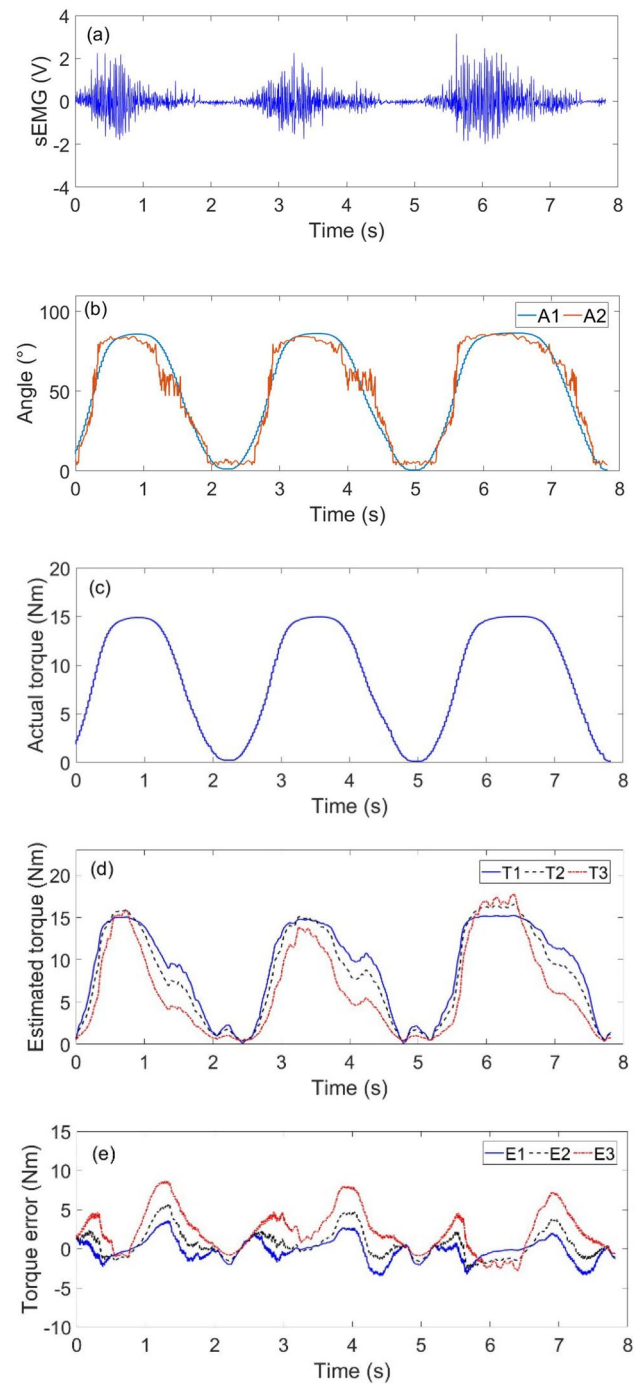


Fig. 10 Above are experimental results under 3 kg load condition. T_1 , T_2 , T_3 represent the estimated torque obtained by Methods 1, 2 and 3, respectively. E_1 , E_2 , E_3 represent errors between actual torque and estimated torque obtained by Methods 1, 2 and 3, respectively. A_1 , A_2 are the actual angle and the estimated angle; **a** Raw sEMG signals **b** Actual angle and estimated angle **c** Actual torque **d** Estimated torque obtained by three estimation strategies **e** Errors between actual torque and three different estimated torques

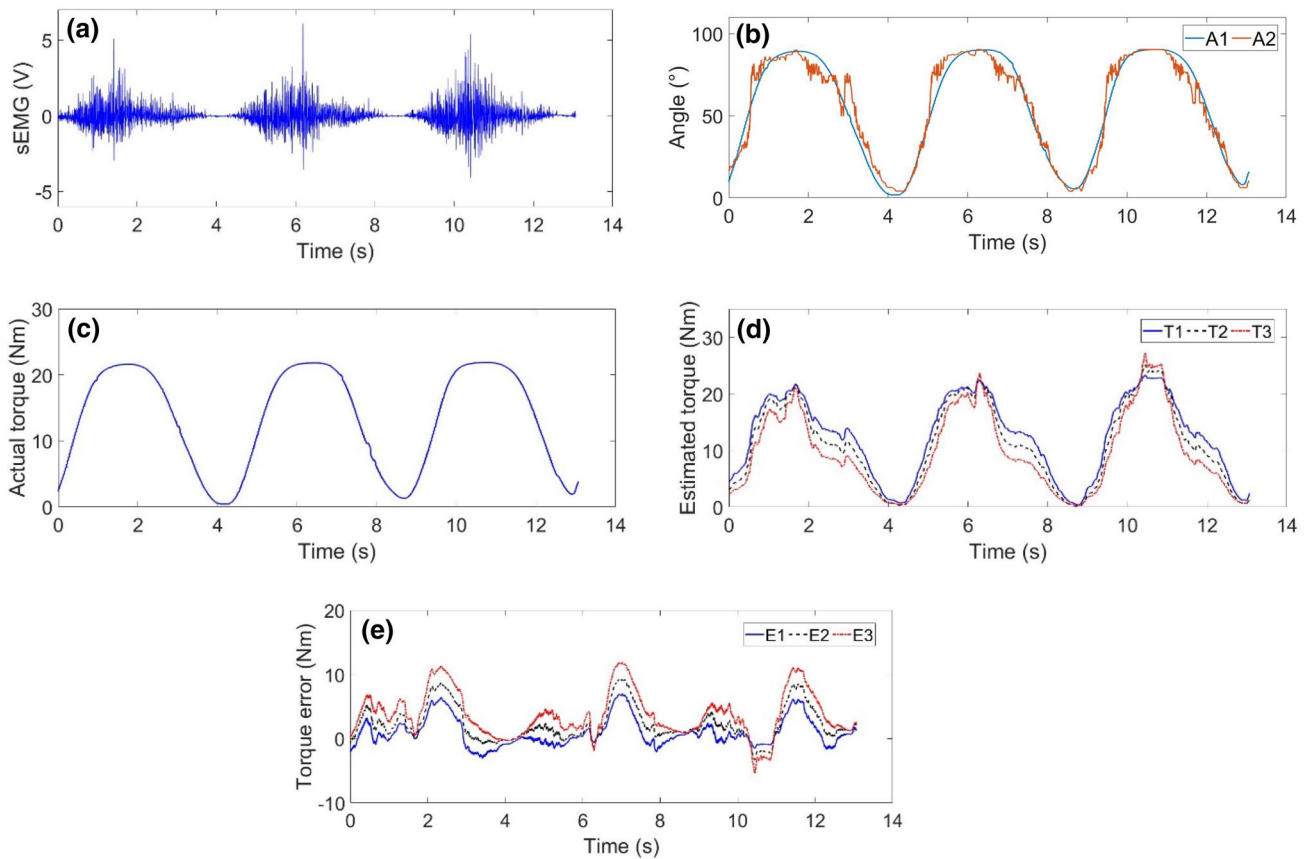


Fig. 11 Above are experimental results under 5 kg load condition. T_1 , T_2 , T_3 represent the estimated torque obtained by Methods 1, 2 and 3, respectively. E_1 , E_2 , E_3 represent errors between actual torque and estimated torque obtained by Methods 1, 2 and 3, respectively. A_1 , A_2 are the actual angle and the estimated angle; **a** Raw sEMG signals **b** Actual angle and estimated angle **c** Actual torque **d** Estimated torque obtained by three estimation strategies **e** Errors between actual torque and three different estimated torque

Table 3 Comparisons of the experimental results obtained by methods 1, 2, 3(M1, M2, M3) AT 1/2 Hz

| | ρ (%) | | | RMSE (Nm) | | | NRMSE (%) | | |
|------|------------|-------|-------|-----------|-------|-------|-----------|--------|--------|
| | M1 | M2 | M3 | M1 | M2 | M3 | M1 | M2 | M3 |
| 0 kg | 93.27 | 92.95 | 89.51 | 3.340 | 6.125 | 4.353 | 13.360 | 24.500 | 17.412 |
| 3 kg | 94.16 | 93.30 | 88.02 | 2.635 | 4.181 | 2.862 | 10.540 | 16.724 | 11.448 |
| 5 kg | 88.50 | 86.42 | 83.15 | 7.007 | 8.045 | 7.816 | 21.897 | 25.141 | 24.425 |

Table 4 Comparisons of the experimental results obtained by methods 1, 2, 3(M1, M2, M3) AT 1/3 Hz

| | ρ (%) | | | RMSE (Nm) | | | NRMSE (%) | | |
|------|------------|-------|-------|-----------|-------|-------|-----------|--------|--------|
| | M1 | M2 | M3 | M1 | M2 | M3 | M1 | M2 | M3 |
| 0 kg | 93.02 | 91.92 | 87.12 | 3.447 | 6.250 | 4.327 | 13.788 | 25.000 | 17.308 |
| 3 kg | 96.68 | 94.74 | 87.35 | 1.914 | 4.760 | 2.487 | 9.550 | 23.800 | 12.435 |
| 5 kg | 92.25 | 91.46 | 88.59 | 6.032 | 8.936 | 6.470 | 18.850 | 27.925 | 20.219 |

big challenge even if the new proposed method can detect muscle changes to a certain extent.

5 Conclusions and Future Works

In order to identify the motion intention, a new torque estimation strategy is proposed in this paper which integrates

Table 5 Comparisons of the experimental results obtained by methods 1, 2, 3 (M1, M2, M3) AT 1/4 Hz

| | ρ (%) | | | RMSE (Nm) | | | NRMSE (%) | | |
|------|------------|-------|-------|-----------|-------|-------|-----------|--------|--------|
| | M1 | M2 | M3 | M1 | M2 | M3 | M1 | M2 | M3 |
| 0 kg | 91.54 | 88.62 | 82.63 | 3.077 | 5.801 | 4.283 | 15.385 | 29.005 | 21.415 |
| 3 kg | 91.68 | 89.51 | 84.68 | 3.813 | 6.007 | 3.835 | 15.252 | 24.028 | 15.340 |
| 5 kg | 87.48 | 85.80 | 78.28 | 7.484 | 8.812 | 7.645 | 23.388 | 27.538 | 23.891 |

sEMG, tension sensor and angle signals to estimate real-time elbow joint torque. Firstly, system identification is proposed to estimate elbow angle, which can be used in the Hill-type muscle model, and replace the use of the angle transducer. In addition, the adaptive adjustment factor is presented to describe the non-linear relationship between sEMG signals and the muscle activation, enabling the estimated torque to be more accurate. Finally, static and dynamic experiments are conducted respectively to verify the improvements of this strategy in terms of torque estimation accuracy.

The purpose of intention recognition is controlling rehabilitation exoskeleton robots and helping patients with hemiplegia to carry out limb rehabilitation training. Thus, developing control strategies based on this torque estimation method to control the rehabilitation exoskeleton robots will be the focus of future works.

Funding This work was supported by the National Natural Science Foundation of China (51705240); the National Natural Science Foundation of Jiangsu (BK20170783); the China Postdoctoral Science Foundation (2018M640480).

Compliance with Ethical Standards

Conflict of interest We declare that we have no financial and personal relationships with other people or organizations that can inappropriately influence our work, there is no professional or other personal interest of any nature or kind in any product, service and/or company that could be construed as influencing the position presented in, or the review of, the manuscript entitled, 'Development of a sEMG-based Joint Torque Estimation Strategy Using Hill-type Muscle Model and Neural Network'.

References

- Chen, Q., Cheng, H., & Huang, R. (2019). Learning and planning of stair ascent for lower-limb exoskeleton systems. *Industrial Robot*, *46*, 421–430.
- Marconi, D., Baldoni, A., & McKinney, Z. (2019). A novel hand exoskeleton with series elastic actuation for modulated torque transfer. *Mechatronics*, *61*, 69–82.
- Wu, Q., Wang, X., & Chen, B. (2018). Development of a minimal-intervention-based admittance control strategy for upper extremity rehabilitation exoskeleton. *IEEE Transactions on Systems, Man, and Cybernetics: Systems*, *48*, 1005–1016.
- Bianchi, M., Cempinib, M., & Contia, R. (2018). Design of a series elastic transmission for hand exoskeletons. *Mechatronics*, *51*, 8–18.
- Wang, M., El-Fiqi, H., & Hu, J. (2019). Convolutional neural networks using dynamic functional connectivity for EEG-based person identification in diverse human states. *IEEE Transactions on Information Forensics and Security*, *14*, 3359–3372.
- Jiang, S., Lv, B., & Guo, W. (2018). Feasibility of wrist-worn, real-time hand, and surface gesture recognition via sEMG and IMU Sensing. *IEEE Transactions on Industrial Informatics*, *14*, 3376–3385.
- Meng, Q., Meng, Q., Yu, H. (2017) A survey on sEMG control strategies of wearable hand exoskeleton for rehabilitation. In *2nd Asia-Pacific Conference on Intelligent Robot Systems, ACIRS* (pp. 165–169).
- Li, Z., Wang, B., & Sun, F. (2014). SEMG-based joint force control for an upper-limb power-assist exoskeleton robot. *IEEE Journal of Biomedical and Health Informatics*, *18*, 1043–1050.
- Duan, F., Dai, L., & Chang, W. (2016). SEMG-based identification of hand motion commands using wavelet neural network combined with discrete wavelet transform. *IEEE Transactions on Industrial Electronics*, *63*, 1923–1934.
- Farina, D., Jiang, N., & Rehbaum, H. (2014). The extraction of neural information from the surface EMG for the control of upper-limb prostheses: Emerging avenues and challenges. *IEEE Transactions on Neural Systems and Rehabilitation Engineering*, *22*, 797–809.
- Noda, T., Furukawa, J. I., Teramae, T. (2013) An electromyogram based force control coordinated in assistive interaction. In *Proceedings—IEEE International Conference on Robotics and Automation*. 3, 2657–2662.
- Xie, H., Huang, H., & Wu, J. (2015). A comparative study of surface EMG classification by fuzzy relevance vector machine and fuzzy support vector machine. *Physiological Measurement*, *36*, 191–206.
- Yao, S., Zhuang, Y., & Li, Z. (2018). Adaptive admittance control for an ankle exoskeleton using an EMG-driven musculoskeletal model. *Frontiers in Neuroinformatics*, *12*, 16.
- Ibitoye, M. O., Hamzaid, N. A., & Abdul Wahab, A. K. (2016). Estimation of electrically-evoked knee torque from mechanomyography using support vector regression. *Sensors (Switzerland)*, *16*, 1–16.
- Gui, K., Liu, H., & Zhang, D. (2019). A practical and adaptive method to achieve EMG-based torque estimation for a robotic exoskeleton. *IEEE/ASME Transactions on Mechatronics*, *24*, 483–494.
- Desplenter, T., & Trejos, A. L. (2018). Evaluating muscle activation models for elbow motion estimation. *Sensors (Switzerland)*, *18*, 1–19.
- Lu, L., Wu, Q., & Chen, X. (2019). Development of a sEMG-based torque estimation control strategy for a soft elbow exoskeleton. *Robotics and Autonomous Systems*, *111*, 88–98.
- Chang, H., Cheng, L., Chang, J. (2017). Development of IMU-based angle measurement system for finger rehabilitation. In *M2VIP 2016—Proceedings of 23rd International Conference on Mechatronics and Machine Vision in Practice*.
- Zhang, Q., Liu, R. W., & Chen, W. (2017). Simultaneous and continuous estimation of shoulder and elbow kinematics from surface EMG signals. *Frontiers in Neuroscience*, *11*, 1–12.

20. Lei, Z. (2019). An upper limb movement estimation from electromyography by using BP neural network. *Biomedical Signal Processing and Control*, *49*, 434–439.
21. Aung, Y. M., & Al-Jumaily, A. (2013). Estimation of upper limb joint angle using surface EMG signal. *International Journal of Advanced Robotic Systems*, *10*, 1–8.
22. Tang, Z., Yu, H., & Cang, S. (2016). Impact of load variation on joint angle estimation from surface EMG signals. *IEEE Transactions on Neural Systems and Rehabilitation Engineering*, *24*, 1342–1350.
23. Artemiadis, P. K., & Kyriakopoulos, K. J. (2006). EMG-based teleoperation of a robot arm in planar catching movements using ARMAX model and trajectory monitoring techniques. In *Proceedings—IEEE International Conference on Robotics and Automation* (pp. 3244–3249).
24. Mamikoglu, U., Nikolakopoulos, G., Pauelsen, M. D. (2016). Elbow joint angle estimation by using integrated surface electromyography. In: *24th Mediterranean Conference on Control and Automation, MED* (pp. 785–790).
25. Sommer, L. F., Barreira, C., Noriega, C. (2018). Elbow joint angle estimation with surface electromyography using autoregressive models. In *Proceedings of the Annual International Conference of the IEEE Engineering in Medicine and Biology Society, EMBS* (pp. 1472–1475).
26. Hudgins, B., Parker, P., & Scott, R. N. (1993). A new strategy for multifunction myoelectric control. *IEEE Transactions on Biomedical Engineering*, *40*, 82–94.
27. Shao, Q., Bassett, D. N., & Manal, K. (2009). An EMG-driven model to estimate muscle forces and joint moments in stroke patients. *Computers in Biology and Medicine*, *39*, 1083–1088.
28. Han, J., Ding, Q., & Xiong, A. (2015). A state-space EMG model for the estimation of continuous joint movements. *IEEE Transactions on Industrial Electronics*, *62*, 4267–4275.
29. Ding, Q. C., Xiong, A. B., Zhao, X. G. (2011). A novel EMG-driven state space model for the estimation of continuous joint movements. In *Conference Proceedings—IEEE International Conference on Systems, Man and Cybernetics* (pp. 2891–2897).
30. Zajac, F. E. (1989). Muscle and tendon: Properties, models, scaling, and application to biomechanics and motor control. *Critical Reviews in Biomedical Engineering*, *17*, 359–411.
31. Holzbaur, K. R. S., Murray, W. M., & Delp, S. L. (2005). A model of the upper extremity for simulating musculoskeletal surgery and analyzing neuromuscular control. *Annals of Biomedical Engineering*, *33*, 829–840.
32. Yang, C., Wang, X., & Li, Z. (2017). Teleoperation control based on combination of wave variable and neural networks. *IEEE Transactions on Systems, Man, and Cybernetics: Systems.*, *47*, 2125–2136.
33. Ghosh-Dastidar, S., Adeli, H., & Dadmehr, N. (2008). Principal component analysis-enhanced cosine radial basis function neural network for robust epilepsy and seizure detection. *IEEE Transactions on Biomedical Engineering*, *55*, 512–518.
34. Wu, Q., Chen, B., & Wu, H. (2019). Neural-network-enhanced torque estimation control of a soft wearable exoskeleton for elbow assistance. *Mechatronics*, *63*, 102279.